forests

MDPI

Article

Variation in the Calyx Color in Two *Styrax japonicus* Varieties Is Attributed to Varied Anthocyanin Levels as Revealed by Integrated Metabolomic and Transcriptomic Analyses

Yiqian Ju [1], Cuiping Zhang [1], Wei Li [1], Cheng Qian [1], Yiming Qu [1], Zhuxiong Zou [2], Han Zhao [3,*,†] and Lulu Li [1,*,†]

[1] College of Landscape Architecture and Forestry, Qingdao Agricultural University, Qingdao 266109, China; juyiqian1991@163.com (Y.J.); zcp116@126.com (C.Z.); weili@qau.edu.cn (W.L.); qauylylxyqc@163.com (C.Q.); 15653591663@163.com (Y.Q.)
[2] Laoshan District Bureau of Nature Resources, Qingdao 266109, China; qdlshzzhx@126.com
[3] Research Institute of Non-Timber Forestry, Chinese Academy of Forestry, Zhengzhou 450003, China
* Correspondence: zhaohan@caf.ac.cn (H.Z.); yuanlinlilulu@126.com (L.L.)
† These authors contributed equally to this work.

Abstract: *Styrax japonicus* is a small ornamental tree with medicinal value. An *S. japonicus* variety with purplish red calyxes and white petals has higher ornamental value. The mechanism underlying calyx pigmentation in *S. japonicus* is still unclear. In this study, metabolome data combined with transcriptome profiling were used to explore the molecular mechanisms underlying the difference in the color of calyx in two varieties of *S. japonicus*, namely, Red Linglong (RA; purplish red calyx) and Green Linglong (GA; green calyx). The Kyoto Encyclopedia of Genes and Genomes (KEGG) enrichment analysis indicated that the levels of delphinidin 3,5-diglucoside, delphinidin 3-O-glucoside, and malvidin 3-O-glucoside when enriched in delphinidin biosynthesis were significantly higher in the RA calyx than in the GA calyx. These key differentially accumulated metabolites were highly correlated with five late biosynthetic genes that were enriched in the anthocyanin biosynthesis pathway. *MYB1*, *MYB82*, and *MYB113* were the three probable transcription factors responsible for anthocyanin accumulation. This study provides novel insights into secondary metabolism pathways, their regulators, and the changes in the transcription and metabolite levels in the calyx of *S. japonicus* regulating sepal color. The results provide a theoretical basis for exploring the mechanism of calyx color formation in *S. japonicus* and provide genetic material and a reference for molecular breeding to obtain desired flower colors in the future.

Keywords: *Styrax japonicus*; anthocyanins; transcriptome; metabolome

check for updates

Citation: Ju, Y.; Zhang, C.; Li, W.; Qian, C.; Qu, Y.; Zou, Z.; Zhao, H.; Li, L. Variation in the Calyx Color in Two *Styrax japonicus* Varieties Is Attributed to Varied Anthocyanin Levels as Revealed by Integrated Metabolomic and Transcriptomic Analyses. *Forests* **2023**, *14*, 1413. https://doi.org/10.3390/f14071413

Received: 3 June 2023
Revised: 2 July 2023
Accepted: 5 July 2023
Published: 11 July 2023

Copyright: © 2023 by the authors. Licensee MDPI, Basel, Switzerland. This article is an open access article distributed under the terms and conditions of the Creative Commons Attribution (CC BY) license (https://creativecommons.org/licenses/by/4.0/).

1. Introduction

Sepals are deformed leaves that form the outermost part of the flower organ in plants. The sepals of a flower, collectively called the calyx, protect the inner body of the flower in the bud. An important role of the calyx is to control flower development and regulate fruit quality [1]. The calyx is usually green. However, in some plants (e.g., lily and magnolia), the calyx is of the same color as the petals and is difficult to distinguish [2,3]. In some groups of plants (e.g., hydrangea and clematis), the calyx appears in various colors, such as blue and pink [4]. In these ornamental plants, the coloration of the calyx is an important ornamental trait and can indicate the pigments that contribute to the color [5].

Anthocyanins are the main determinant of coloration in floral organs. As a branch of the flavonoid biosynthesis pathway [6], anthocyanin biosynthesis is catalyzed by a series of enzymes that are encoded by early biosynthetic genes (EBGs) [such as *chalcone synthase* (*CHS*), *chalcone isomerase* (*CHI*), *flavanone 3-hydroxylase* (*F3H*), and *flavanone 3′-hydroxylase* (*F3′H*)] and late biosynthetic genes (LBGs) [such as *dihydroflavonol-4-reductase*

(*DFR*), *anthocyanidin synthase* (*ANS*), and *flavonoid 3-O-glucosyltrnsferase* (*UFGT*)] [7,8]. At the late biosynthesis term, the immediate precursors of anthocyanins can also be catalyzed by leucoanthocyanidin reductase (LAR) and anthocyanidin reductase (ANR) to synthesize proanthocyanidins (PAs), which are directed to the branches of other flavonoid substances [9].

The structural genes encoding enzymes of the anthocyanin and PA synthesis pathways are generally regulated by transcription factors (TFs) at the transcription level [10]. Many studies have reported that R2R3-MYB TFs play an important role in anthocyanin accumulation. Among the R2R3-MYB TFs, the R2R3-MYB activators (such as *AtMYB75*, *AtMYB90*, *AtMYB113*, and *AtMYB114*) and R2R3-MYB repressors (such as *FaMYB1-type* and *PpMYB18-type* MYB TFs) play essential roles in regulating the anthocyanin accumulation [9,11,12]. The R2R3-MYB TFs generally interact with a basic helix–loop–helix (bHLH) and WD40-repeat proteins to form a MBW protein complex when regulating the expression of structural genes enriched in the anthocyanin biosynthesis pathway [13,14]. The GL3, EGL3, TT8, and PIFs are bHLH proteins that were reported to be the second major TF-regulating genes involved in anthocyanin synthesis [15–17]. In *Centaurea cyanus*, CcMYB6-1 interacted with CcbHLH1, regulating the gene expression of *CcF3H* and *CcDFR* to stimulate anthocyanin accumulation [18]. In *Arabidopsis*, PIF4 interacted with PAP1, negatively regulating the anthocyanin accumulation, and could compete with TT8 to bind to PAP1 [19]. In certain model plants, many negative regulators, such as MYBL2, PIF4, PIF5, and NAC TFs, inhibit anthocyanin accumulation by interacting with members of MBW [20–23]. A recent study involving the integrated analysis of transcriptome and metabolome in flowers and fruits reported changes in the levels of secondary metabolites and corresponding differential gene expressions [24,25], enhancing an understanding of flower color regulation in plants.

Styrax japonicus, with luxuriant and fragrant flowers, is an important ornamental plant in spring and summer gardens and is widely distributed across East Asian countries. After flowering, the slender pedicel connected to the funnel-shaped calyx made the corolla pendulous. The color of the calyx and pedicel in normal flowers is generally green, and color mutations are infrequent in *S. japonicus*. Due to natural variation and during the process of adaptation to new environments, a few specific individual plants of *S. japonicus* exhibited a purplish red color in the calyx and pedicel. The contrast between the purplish red sepals and white petals greatly enhanced their ornamental value. Therefore, these seedlings are largely cultivated to obtain newer varieties. Previous bioinformatic studies on *S. japonicus* have only focused on the flowering-associated genes and the development of simple sequence repeat markers [26–28]. The candidate genes and pathways responsible for the anthocyanin accumulation in *S. japonicus* have not been reported to date.

In the current study, we comparatively analyzed the metabolome and transcriptome of calyxes from two different varieties of *S. japonicus*, namely, Green Linglong (GA; green calyx) and Red Linglong (RA; red calyx) (Figure 1), to understand the mechanisms underlying the difference in the color of sepals between GA and RA. Some differentially expressed genes involved in calyx pigmentation were identified, and the corresponding candidate metabolites were revealed. This study aimed to enhance our understanding of the gene regulatory mechanisms and biological pathways involved in anthocyanin accumulation in *S. japonicus*, laying a foundation for future investigations regarding resource development and the molecular breeding of *S. japonicus.*



Figure 1. Flowers of *Styrax japonicus* 'Green Linglong' (GA) and *S. japonicus* 'Red Linglong' (RA). (**A**) GA. (**B**) RA.

2. Materials and Methods

2.1. Plant Materials

The calyxes of two types of *S. japonicus*, namely, Green Linglong (GA; green calyx) and Red Linglong (RA; red calyx), were collected from Shandong Provincial Center of Forest and Grass Germplasm Resources, Licheng District, Jinan, China (36.63° N, 117.20° E). These experiments involved three biological replicates of each type of calyx. The three replicate samples of the GA calyx were numbered GA1, GA2, and GA3, and those of the RA calyx were numbered RA1, RA2, and RA3. Each biological replication involved 25 randomly collected calyxes. All the fresh samples were immediately frozen in liquid nitrogen and stored at −80 °C until further use.

2.2. Calyx Color Measurement

Approximately 30 fully pigmented calyxes were randomly sampled. These fresh calyxes were immediately used to determine the values of L*, a*, and b* by a chroma meter (NF555, Nippon Denshoku Industries Co., Ltd., Tokyo, Japan) [29]. Ten technical replicates were conducted and analyzed as one biological replicate.

2.3. Assessment of Total Flavonoid and Anthocyanin Contents

The ultraviolet spectrum analysis of anthocyanidins and flavonoids was performed. In total, 0.1 g of calyx powder was added to 2 mL of 1% hydrochloric methanol. The suspension was incubated in the dark at 25 °C for 24 h and filtered through a 0.22-μm membrane. The filtered liquid was diluted to make up a volume of 10 mL using 1% hydrochloric methanol. The absorbance of this liquid was measured at 220–600 nm by an Agilent Cary 60 UV-visible spectrophotometer (Agilent Technology Co., Ltd., Shanghai, China).

The flavonoids were extracted as per the protocol described in a previous study by Pekal [30]. Calyxes (0.5 g) were ground into powder in liquid nitrogen. To this powder, 50 mL of 10% ethanol (Shanghai, China) was added. The mixture was heated in a water bath for 20 min, transferred to a 100-mL volumetric bottle, and diluted with 10% ethanol solution to 100 mL. Further, the liquid was passed through a 0.22-μm syringe filter into the sample bottles to obtain a flavonoid extract. The absorbance of the extract was measured at 510 nm. A Rutin (quercetin-3-rutinoside) solution (BW1681, Beijing Wanjia Biotechnology Co., Ltd., Beijing, China) was used as the standard solution. The total flavone content was calculated according to the standard curve [31].

The total anthocyanin content was calculated as described by Wang (2018) [32]. In total, 0.1 g of calyx powder was dissolved in 10 mL of a 0.1 mol/L hydrochloric acid

ethanol solution, and the extraction was conducted at 60 °C for 30 min. To this, 5 mL of 0.1 mol/L hydrochloric acid ethanol solution was added, and incubation was continued for 30 min. The volume of the liquid was made up to 25 mL using a 0.1 mol/L hydrochloric acid ethanol solution. The experiment was performed in triplicates. The absorbance of the liquid was measured at 530, 620, and 650 nm.

2.4. Measurement of Cell Sap pH

Fresh GA and RA calyxes were carefully collected. The pH of the cell sap was determined as described by Qi et al. [33] using a pH meter (PHS-3C, Inesa Scientific Instrument Ltd., Shanghai, China). The experiment involved 6 biological replicates.

2.5. Extraction of Secondary Metabolites

The freeze-dried calyx samples were crushed at 30 Hz for 1.5 min using a mixer mill (MM 400, Retsch) with zirconia beads. The resulting powder (100 mg) was mixed with 1.0 mL 70% aqueous methanol and was subjected to an overnight extraction at 4 °C. Further, the solutions were centrifuged at 10,000× g for 10 min. The supernatant was filtered and subjected to LC-MS analysis using the LC-ESI-MS/MS system (UPLC, Shim-pack UFLC SHIMADZU CBM30A system; MS/MS, Applied Biosystems 6500 QTRAP). For each sample, 2-µL of aliquot was injected into the Waters ACQUITY UPLC HSS T3 C18 column (1.8 µm, 2.1 mm × 100 mm) with a flow rate of 0.4 mL/min. The binary solvent system was established as described by Wang et al. (2017) [34].

2.6. Identification and Quantification of Metabolites

The identification and quantification of metabolites were performed as previously described [35,36]. Based on the self-built MWDB (metware database) and public databases of MoTo DB (http://www.ab.wur.nl/moto/, accessed on 10 October 2019), MassBank (http://www.massbank.jp/, accessed on 10 October 2019), and METLIN (http://metlin.scripps.edu/index.php, accessed on 10 October 2019), the metabolites were identified and annotated. The metabolites were quantified using multiple reaction monitoring (MRM). The identified metabolites were subjected to an orthogonal partial least square-discriminate analysis (OPLS-DA). The DAMs were screened based on the FC and VIP value of OPLS-DA. Metabolites with a VIP value ≥ 1 and FC ≥ 2 or FC ≤ 0.5 were considered DAMs. The DAMs were mapped to the KEGG pathway database (http://www.kegg.jp/4eg/pathway.html, accessed on 1 November 2019) for the enrichment analysis of pathways and the further identification of key pathways.

2.7. Transcriptome Analysis

The total RNA was extracted from the calyxes of GA and RA (DP441, TIANGEN biochemical Technology Co., Ltd., Beijing, China). cDNA library construction and sequencing were performed as reported previously [37]. Sequencing libraries were generated using the NEBNext® Ultra™ RNA Library Prep Kit for Illumina® (NEB, Ipswich, MA, USA). The Illumina HiSeq™ 2000 platform was used for sequencing. The experiment involved three biological replicates.

The transcriptome assembly was constructed using Trinity [38]. The unigenes were functionally annotated using various protein databases. The gene expression level was normalized to the FPKM values. The DEGs were filtered by applying the DESeq algorithm with $|\log_2 FC| \geq 2$ and a false discovery rate (FDR) < 0.05. The identified DEGs were further subjected to GO enrichment analysis and KEGG pathway analysis. The TFs were predicted using the iTAK program (http://itak.feilab.net/cgi-bin/itak/index.cgi, accessed on 10 January 2020).

2.8. RT-qPCR Verification

To validate the levels of gene expression, as reflected by the FPKM values, 10 transcripts were selected and subjected to RT-qPCR. GAPDH and PP2A were used as the

reference genes [39]. The PCR was performed as described previously [28]. The relative abundance of the selected transcripts was analyzed using the $2^{-\Delta\Delta Ct}$ method.

2.9. Association Analysis of Metabolome and Transcriptomic Profiling

According to the results of metabolome and transcriptome analyses, the DEGs and DAMs in the same group were simultaneously mapped to the KEGG pathway map to further understand the relationship between the genes and metabolites. In this experiment, Log_2 transformation was uniformly performed on the data before analysis. Correlation coefficient values were calculated to analyze the association between significant DEGs and DAMs. The screening criteria for the results were Pearson's correlation coefficient > 0.9.

2.10. Statistical Analysis

The statistical analyses were performed using SPSS 17.0 software (IBM SPSS, Chicago, IL, USA). The correlation heatmap and co-expression analysis were conducted using a network analysis platform (https://www.omicstudio.cn/index, accessed on 3 May 2020).

3. Results

3.1. Analysis of Color Phenotype in the GA and RA Calyxes

Chroma values were used to quantify the color of the sepals. The a* values ranged from −10.78 (GA) to 22.93 (RA). The b* values ranged from 3.68 (RA) to 38.72 (GA). The L* value of the RA calyx was significantly lower ($p < 0.05$) than that of the GA calyx (Figure 2).

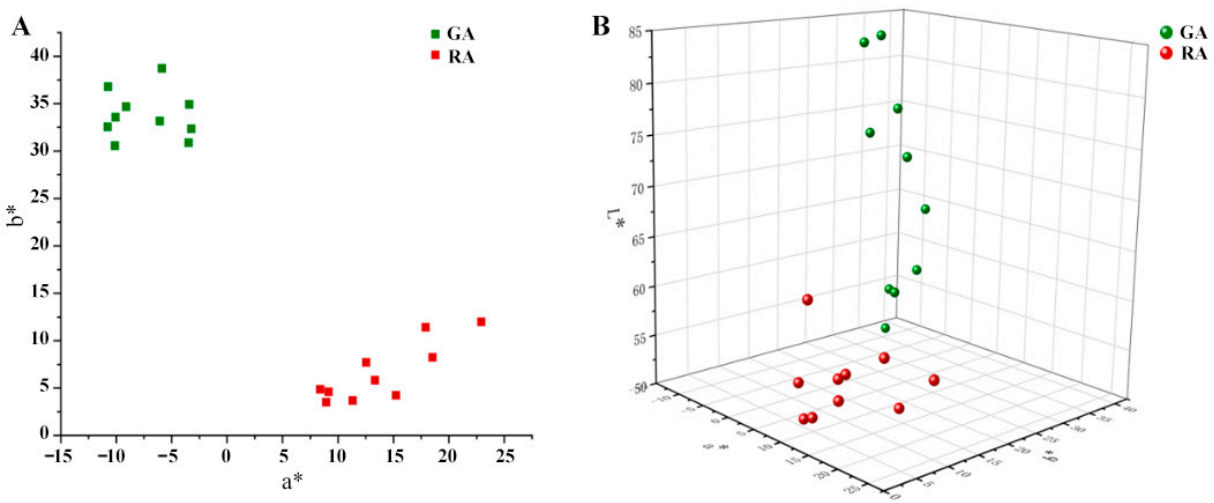


Figure 2. L*, a*, and b* paraments of calyxes GA and RA. (**A**) a* and b* paraments of calyxes GA and RA. (**B**) Three-dimensional diagram of L*, a*, and b* paraments.

3.2. Pigment Components of the GA and RA Calyxes

Two clear absorption peaks were obtained at 230–380 nm in the pigment extracts of the GA and RA calyxes, indicating that both calyxes contained flavonoids (Figure 3A). The pigment extracts of the RA calyx exhibited a clear absorption peak of anthocyanins at approximately 550 nm, whereas those of the GA calyx exhibited no clear absorption peak, indicating that the main pigment components of the RA calyx were anthocyanins (Figure 3B).

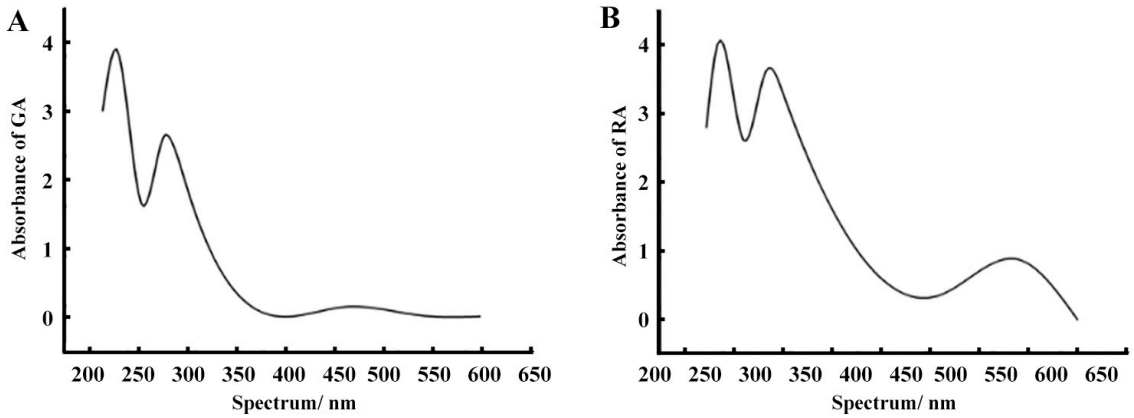


Figure 3. Ultraviolet-visible spectrum analysis of pigment components. (**A**) Absorbance of GA calyxes. (**B**) Absorbance of RA calyxes.

3.3. Content of Flavonoids and Anthocyanins in the GA and RA Calyxes

The content of the total flavonoids in the samples was determined using the $AlCl_3$ color-developing method. The total flavonoid content in the RA and GA calyxes was 60 ± 1.25 and 45 ± 2.54 mg/g, respectively (Figure 4A), and was not significantly different ($p > 0.05$). The anthocyanin content in the RA calyxes was considerably higher (by more than twice) than that in the GA calyxes. This indicated that the main reason underlying the color difference in the GA and RA calyxes could be significantly different from the anthocyanin content (Figure 4B).

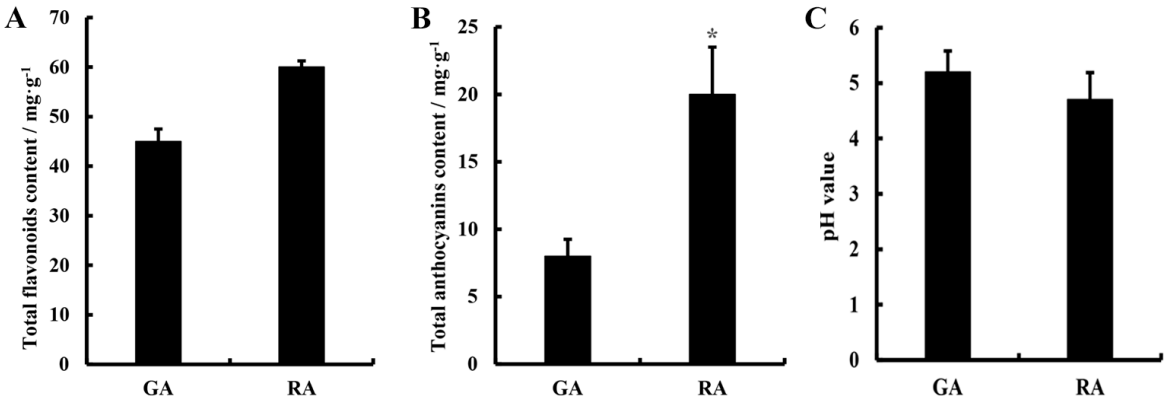


Figure 4. Identification of pigment contents and pH values in calyxes of GA and RA. (**A**) Total flavonoid content in calyxes of GA and RA. (**B**) Total anthocyanins content in calyxes of GA and RA. (**C**) pH values for the calyx sap of GA and RA. Asterisk "*" represents significance levels at $p < 0.05$.

3.4. Analysis of Sap pH

To assess the effect of pH on the calyx color, the sap pH of RA and GA calyxes was measured, and this was observed to be 4.7 ± 0.49 and 5.2 ± 0.38, respectively (Figure 4C). However, the pH values were not significantly different between the GA and RA calyxes.

3.5. Analysis of Differential Metabolites in the GA and RA Calyxes

The metabolites in the GA and RA calyxes were compared to study the differential metabolites that were responsible for the pigmentation of the GA and RA calyxes. In total, 828 metabolites were detected from six samples using UPLC-ESI-QTRAP-MS/MS and MRM. The datasets were subjected to principal component analysis (PCA) with a 3D scatter plot. PC1 (51.35%), PC2 (12.3%), and PC3 (10.17%) were extracted with a cumulative contribution rate of 73.82%, which indicated significant metabolic differences between the calyxes of the two varieties and a good identity among the replicates (Figure S1A).

These results indicate that the experiment was reliable and reproducible. A hierarchical heatmap clustering analysis (HCA) of all the samples was performed. The two varieties were grouped separately, suggesting the high reliability of metabolic data (Figure S1C).

The OPLS-DA is more conducive for the screening of differential metabolites because of its capability to maximize the distinction between treatments. In this study, the OPLS-DA model was used to compare the content of metabolites that were present in the samples to assess the difference between the GA and RA calyxes, where the R^2X, R^2Y, and Q^2 values were 0.918, 1, and 0.998, respectively (Figure S1B). These results indicate that the model was meaningful and stable and could be used for the screening of differential metabolites in the subsequent analysis.

A combination of variable importance in projection (VIP) and fold change (FC) was used for the screening of differentially accumulated metabolites (DAMs). A total of 202 DAMs were identified with 115 up- and 87 downregulated metabolites in the RA calyx vs. the GA calyx (Table S1, Figure S1D). The main DAMs were flavonoids (71; 35.15%) and anthocyanins (21; 10.40%), followed by quinate and its derivatives (14; 6.93%), hydroxycinnamoyl derivatives (13; 6.44%), phenolamides (12; 5.94%), and organic acids (11; 5.45%) (Figure S1E).

Seven types of anthocyanins, including petunidin, peonidin, pelargonin, malvidin, delphinidin, cyaniding, and cyanin, were identified in the GA vs. RA. As shown in Figure 5A, the top eight upregulated metabolites contained six anthocyanins [including delphinidin 3,5-diglucoside (log_2FC = 20.79), delphinidin 3-O-glucoside (log_2FC = 10.02), malvidin 3-O-glucoside (log_2FC = 9.94), malvidin 3,5-diglucoside (log_2FC = 9.14), malvidin 3-O-galactoside (log_2FC = 8.88), and malvidin 3,5-diglucoside (log_2FC = 8.13)], one quinate and its derivative (5-O-p-coumaroyl shikimic acid O-hexoside), and one organic acid (lithospermic acid). Three anthocyanins, namely, pelargonin (log_2FC = −19.36), cyanidin 3,5-O-diglucoside (log_2FC = −15.91), and cyanidin O-acetylhexoside (log_2FC = −11.50) were present in the top 10 downregulated metabolites. The results indicate that upregulated metabolites such as delphinidin and malvidin might be responsible for the pigmentation in the red calyx of RA.

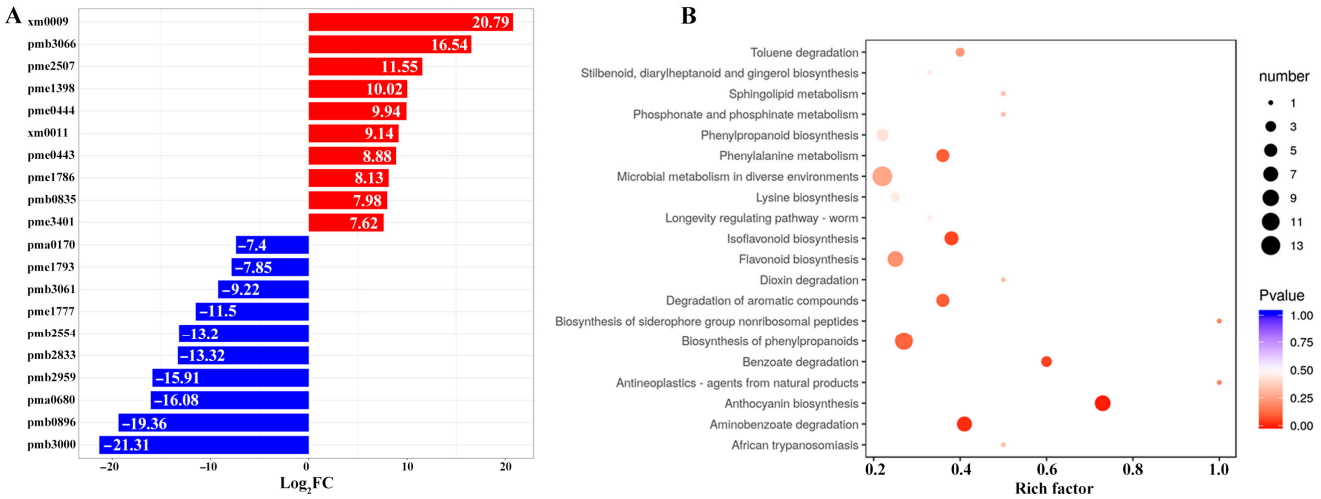


Figure 5. Analysis of differentially accumulated metabolites (DAMs) in GA and RA. (**A**) Top 20 FC change metabolites of up- and down- regulated DAMs. (**B**) Statistics of top 20 KEGG enrichment pathways of up- and down-regulated DAMs.

The enriched KEGG terms of the DAMs in the GA calyx vs. RA calyx were obtained. The top five enrichment pathways were anthocyanin biosynthesis (ko00942), aminobenzoate degradation (ko00627), benzoate degradation (ko00362), isoflavonoid biosynthesis (ko00943), and the degradation of aromatic compounds (ko01220) (Figure 5B, Table S2). A total of eight DAMs annotated to the anthocyanin biosynthesis pathway exhibited a very significant enrichment effect and remarkably different FC. Of the eight DAMs, four

DAMs that were annotated to the branch of delphinidin might be the key compounds responsible for the pigmentation of the RA calyx. The upstream biosynthetic pathways for anthocyanins were the phenylpropanoid and flavonoid pathways, to which four and seven DAMs were annotated, respectively (Table S3). Of these DAMs, cinnamic acid (pme0299) in the phenylpropanoid pathway and five DAMs including dihydrokaempferol (DHK, pme2963), dihydroquercetin (DHQ, pme1521), myricetin (pme1478), epigallocatechin (EGC, pme1514), and gallocatechin (GC, pme1537) in the flavonoid pathway were associated with anthocyanin accumulation.

3.6. Transcriptome Analysis of the Calyxes

To identify the genes involved in calyx coloration, RNA-seq analysis was performed using six cDNA libraries derived from the calyxes, which were also used for the metabolite profiling analysis. A total of 152,839,364 clean reads were generated and were de novo assembled to obtain the reference sequences (Table S4). The length distributions of the assembled transcripts and unigenes are presented in Table S5. The total clean reads were mapped to the reference sequences with match ratios ranging from 74.91% to 75.39% (Table S6). In total, 352,415 unigenes were expressed in the calyxes. PCA analysis indicated high correlation coefficients within the groups and considerable differences between the groups (Figure S2A). The number of differentially expressed genes (DEGs) was 4945, including 2517 up- and 2428 down-regulated DEGs in the GA calyxes (Figure S2B, Table S7). The clustered patterns of all DEGs indicated the differential expression patterns between the two calyxes (Figure S2C).

GO analysis was performed, and the DEGs were assigned to 23 biological process categories, 13 cellular components categories, and 9 molecular function categories (Figure S2D). In the biological process, the "cellular process" and "metabolic process" were the first two large subgroups. The various metabolite-related enriched terms suggested that the metabolic function could be closely related to the change in the color of the calyx. To identify the potential biological pathway, DEGs were subjected to KEGG pathway enrichment analysis. Five categories were assigned by 863 DEGs that were enriched to 257 KEGG pathways. Most DEGs (279 DEGs) were annotated with metabolic pathways, followed by the biosynthesis of secondary metabolites (174 DEGs) (Figure S2F, Table S8). Among the top 20 KEGG pathways, the "Ras signaling pathway" (ko04014), "Photosynthesis—antenna proteins" (ko00196), "Flavonoid biosynthesis" (ko00941), and "Plant-pathogen interaction" (ko04626) were the most significantly enriched pathways. The phenylpropanoid biosynthesis pathway (ko00940), which is the upstream pathway of the flavonoid, and anthocyanin were also significantly enriched (Figure S2E, Table S9). These results suggest that the metabolic processes related to anthocyanin accumulation mainly affected the change in calyx color.

A total of 52 DEGs enriched in the biosynthetic pathways of phenylpropanoid, flavonoid, and anthocyanin were determined. Of these, 16 DEGs which encoded key enzymes involved in anthocyanin biosynthesis were identified; these mainly included two phenylalanine ammonialyase (*PAL*) genes, four flavonol synthase (*FLS*) genes, six anthocyanidin synthase (*ANS*) genes, two dihydro-flavonol 4-reductase (*DFR*) genes, one leucoanthocyanidin reductase (*LAR*) gene, and one UDP-glucose flavonoid transferase (*UFGT*) gene (Table S10). Most of these DEGs exhibited higher transcript levels in the RA calyx than in the GA calyx. This could explain, at least partially, the higher level of anthocyanin accumulation in the RA calyx than in the GA calyxes. It is worth noting that the expressions of *LAR* (DN95067_c0_g3) in the catechin biosynthesis pathway and *FLS* (DN99414_c1_g1) in the flavonol biosynthesis pathway were downregulated by more than 9.0- and 7.7-fold, respectively.

In total, 69 differentially expressed TFs were obtained, with 49 up- and 20 down-regulated TFs in the GA calyx (Figure S3, Table S11). Five MYBs and two bHLHs were potentially involved in anthocyanin biosynthesis, and TFs with $|\log_2 FC| \geq 7$ were selected for co-expression analysis with the above 16 differentially expressed structural genes. Overall, four MYB-related genes (*MYB1*: *DN89812_c3_g1*, *DN94375_c1_g1*, *MYB82*:

DN78431_c4_g4, and *MYB113*: *DN66235_c0_g2*), two bHLHs (*PIF3*: *DN82050_c1_g1* and *MYC2*: *DN102308_c2_g1*), GRAS (*DELLA*: *DN103810_c1_g1*), AP2/ERF-ERF (*PTI6*: *DN83232_c0_g2*), and C2C2-Dof (*CDF1*: *DN100839_c2_g1*) exhibited a high correlation degree with eight structural genes related to anthocyanin synthesis, including *UFGT* (*DN92718_c0_g1*), *FLS* (*DN87815_c2_g2*), *ANSs* (*DN87815_c2_g1*, *DN102834_c0_g1*, *DN93280_c6_g2* and *DN90681_c0_g1*), *DFR* (*DN103348_c0_g1*), and *LAR* (*DN95067_c0_g3*) in the calyx of *S. japonicus* (Figure 6A). The correlation heatmap indicated that three MYB-related genes (*MYB82*, *DN94375_c1_g1*, and *MYB113*), *DELLA*, *MYC2*, and *CDF1*, were positively correlated with the above seven structural genes and negatively correlated with *LAR*. Noticeably, *MYB1*, *PTI6*, and *PIF3* exhibited the exact opposite trend in regulating the eight structural genes in *S. japonicus* (Figure 6B). The results suggest that these eight DEGs were enriched in the anthocyanin biosynthesis pathway and flavonoid biosynthesis pathway as the key candidate genes involved in anthocyanin synthesis and could be regulated by specific TFs. This could be responsible for the differential anthocyanin accumulation between the GA and RA calyxes.

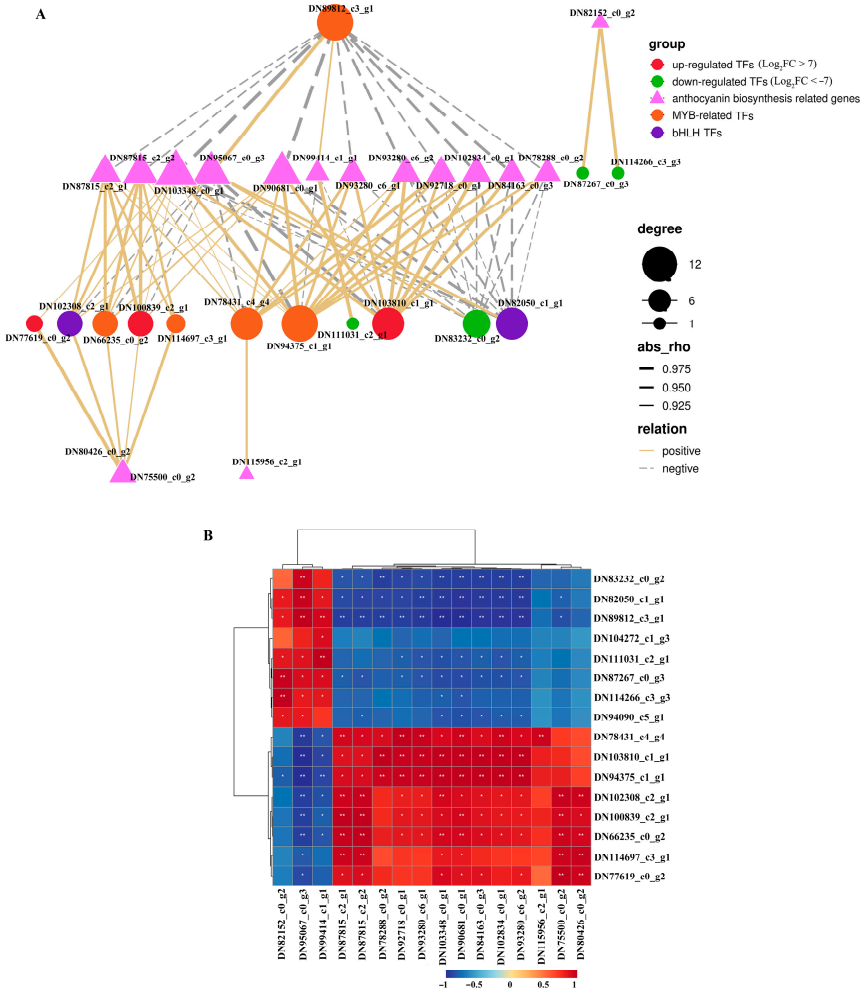


Figure 6. Correlation analysis of transcription factors (TFs) with $|\log_2 FC| \geq 7$, MYBs, bHLHs, and differentially expressed structural genes related to anthocyanin biosynthesis. (**A**) The co-expression analysis of TFs with $|\log_2 FC| \geq 7$, MYBs, bHLHs, and differentially expressed structural genes relating to anthocyanin biosynthesis. The R was more than 0.9 and less than −0.9 with $p < 0.05$. (**B**) The correlation heatmap of TFs with $|\log_2 FC| \geq 7$, MYBs, bHLHs, and differentially expressed structural genes were related to anthocyanin biosynthesis. Asterisks "*" and "**" indicate significance levels at $p < 0.05$ and $p < 0.01$, respectively.

The relative expression levels of 12 anthocyanin-related genes were analyzed using qPCR to validate the transcriptome results. Their expression patterns were generally consistent with the RNA-Seq results (Figure S4).

3.7. Correlation Analysis of Metabolites and Transcripts Involved in Anthocyanin Accumulation in the Two Types of Calyxes

For a better explanation of the relationship between metabolites and genes in anthocyanin accumulation in the calyxes, we established a network based on 4945 DEGs and 202 DAMs to describe the relationship between the metabolite accumulation and differential gene expression (Figure S5). The co-expression analysis indicated a high correlation among all DEGs and DAMs.

A pathway map containing metabolites and structural genes relating to anthocyanin biosynthesis was constructed based on the enriched KEGG databases (Figure 7A). The DEGs and DAMs were mainly enriched in the flavonoid and anthocyanin biosynthesis pathways. The expression of *PAL* (DN78288_c0_g2), three *FLSs*, three *DFRs*, six *ANSs*, and one *UFGT* in RA was significantly higher than that in the GA calyx. The expression of *LAR* was significantly downregulated in the RA calyx. Early metabolites such as DHK (pme2963) and DHQ (pme1521) exhibited significantly higher levels in the RA calyx. The levels of one anthocyanin (cyanidin, pme3609) and two catechin derivatives (gallocatechin, pme1537, and epigallocatechin, pme1514) were significantly decreased in the calyx of RA. In the late stage of anthocyanin biosynthesis, the levels of cyanidin 3,5-O-diglucoside (pme1777) and pelargonidin 3,5-diglucoside (pme1793) were downregulated by more than 15- and 19-folds, respectively. The levels of delphinidin derivatives such as delphinidin 3,5-diglucoside (xm0009), delphinidin 3-O-glucoside (pme1398), petunidin 3-O-glucoside (pme3391), and malvidin 3-O-glucoside (pme0444) were significantly higher in the RA calyx than those in the GA calyx, which suggests that the calyx color of RA was mainly related to the delphinidin derivatives.

To understand the relationship between anthocyanin-related genes and metabolites, correlation tests were conducted. The correlation network revealed that eight differentially expressed structural genes and nine TFs were co-expressed with 18 anthocyanin-related metabolites. Of the 17 DEGs, *UFGT* (*DN92718_c0_g1*), three *ANSs* (*DN102834_c0_g1*, *DN93280_c6_g2* and *DN90681_c0_g1*), *DFR* (*DN103348_c0_g1*), *LAR* (*DN95067_c0_g3*), four MYB-related genes (*MYB1*: *DN89812_c3_g1*, *DN94375_c1_g1*, *MYB82*: *DN78431_c4_g4* and *MYB113*: *DN66235_c0_g2*), bHLH (*PIF3*: *DN82050_c1_g1*), GRAS (*DELLA*: *DN103810_c1_g1*), and AP2/ERF-ERF (*PTI6*: *DN83232_c0_g2*) were highly correlated with the metabolites. *UFGT*, three *ANSs*, *DFR*, *DELLA*, and the *MYB*-related gene (*DN94375_c1_g1*) were positively correlated with the levels of delphinidin and malvidin derivatives and negatively correlated with the levels of cyanidin and pelargonidin derivatives. *LAR*, *MYB1*, *PTI6*, and *PIF3* exhibited an opposite trend (Figure 7B).

Collectively, the comparison between transcriptome and metabolome indicated the same trend of change in the expression of DEGs and DAMs in relation to anthocyanins and their derivatives. Therefore, it was speculated that the delphinidin and malvidin derivatives were the main metabolites affecting the calyx color in the two varieties of *S. japonicus*.

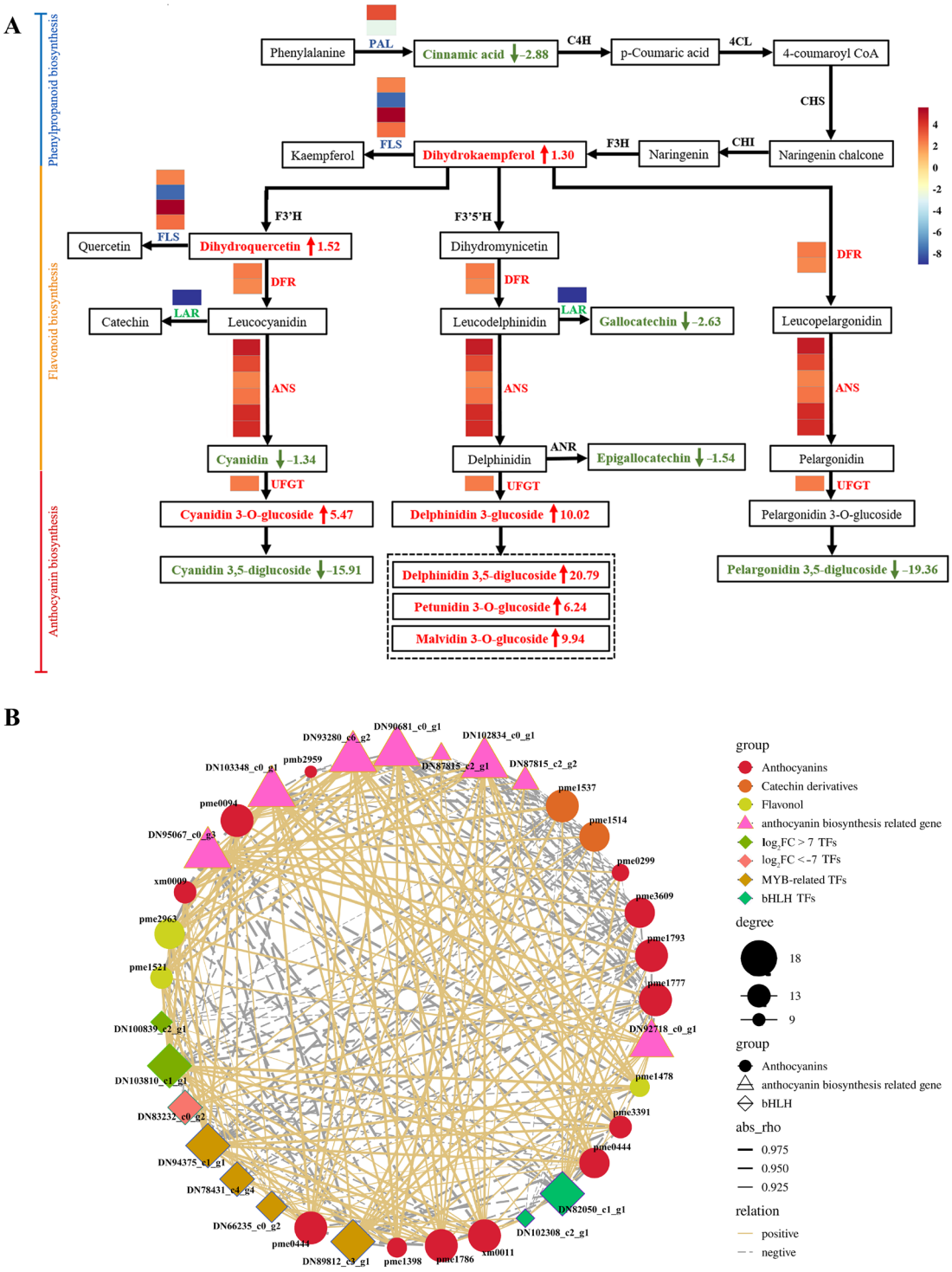


Figure 7. Analysis of TFs, DEGs, and DAMs in relation to anthocyanin biosynthesis. (**A**) The pathway map containing DAMs and DEGs in relation to anthocyanin biosynthesis. (**B**) The co-expression analysis of TFs, DEGs, and DAMs in relation to anthocyanin biosynthesis. R was more than 0.9 and less than −0.9 with $p < 0.05$.

4. Discussion

4.1. Anthocyanins Are Differentially Expressed in the Calyxes of S. japonicus

S. japonicus is a member of the Styracaceae family. It is a deciduous tree species. The wild-type *S. japonicus* has green sepals with white bell-shaped flowers, whereas the other variety (RA) contains purplish red sepals and has a high ornamental value. Previous

research has shown that the main components that determine the coloration in plants are some secondary metabolites belonging to the class of flavonoids, among which anthocyanins are responsible for various vivid colors from red to purple and blue [40]. However, the genetic basis and chromogenic mechanism of calyx coloration in RA is still unclear. Combined transcriptomic and metabolomics analyses could provide more information on the dynamic metabolic changes and regulatory mechanisms underlying calyx pigmentation in *S. japonicus*.

Research has indicated that various anthocyanin chromophores are the primary contributors to color phenotypes. In some species that have more than one color in their flower, the color variation is also linked to vacuolar pH differences [28]. In our study, no significant difference was observed in the vacuolar pH of calyxes between GA and RA. The purplish red calyx pigmentation in RA was mainly due to the hyperaccumulation of anthocyanins. A previous study reported that dark-colored calyxes have a higher content of anthocyanins, and white or green calyxes lack these flavonoids or have minimal quantities [41,42]. An analysis of the top 10 upregulated metabolites indicated that two delphinidin derivatives and four malvidin derivatives were significantly and highly accumulated in purplish red calyxes. KEGG enrichment analysis suggested that the purplish red color of the calyxes of *S. japonicus* could be attributed to delphinidin 3,5-diglucoside ($log_2FC = 20.79$), delphinidin 3-O-glucoside ($log_2FC = 10.02$), and malvidin 3-O-glucoside ($log_2FC = 9.94$), which were all annotated in the branch of delphinidin biosynthesis. Delphinidin has been reported to be a purple-colored plant pigment that is present in various flowers and fruits [43,44]. In some Asian dark-purple tea cultivars, a large number of delphinidin-related anthocyanins are accumulated [45]. In addition to delphinidin, malvidin has also been reported as a major component in some African violet tea cultivars [46]. Anthocyanins are water-soluble and beneficial to human health. In recent years, the medical values of various parts of *S. japonicus*, including stem bark, fresh fruits, and flowers, have been investigated [47]. The medicinal properties of this variant with purplish red calyx are suggested for future study.

4.2. Anthocyanin Accumulation in the Calyx of S. japonicus May Be Influenced by a Series of Metabolic Pathways

The difference in anthocyanin synthesis and accumulation could be due to various factors. However, the difference in the expression of EBGs or LBGs plays an important role in this. In the present study, 52 DEGs encoding enzymes involved in anthocyanin accumulation were identified using KEGG enrichment analysis. The correlation analysis of the metabolites and transcripts indicated that *UFGT* (*DN92718_c0_g1*), three *ANSs* (*DN102834_c0_g1*, *DN93280_c6_g2,* and *DN90681_c0_g1*), and *DFR* (*DN103348_c0_g1*) were the important genes encoding the enzymes that played important roles in the modulation of the delphinidin derivative biosynthesis in *S. japonicus*. This suggests that the different expression mechanisms of LBGs during anthocyanin biosynthesis resulted in the different pigmentation of the GA and RA calyxes.

The KEGG pathway enrichment analysis revealed that the structural genes in anthocyanin-related pathways and the DEGs enriched in other pathways exhibited a differential expression in the GA and RA calyxes. This suggested that the differences in anthocyanin accumulation might also be related to other metabolic pathways in the calyxes of *S. japonicus*. A total of 12 DEGs were annotated in the "Photosynthesis—antenna proteins" pathway. This indicated that the photosynthetic properties were different in GA and RA. Previous studies have reported that the signals that stimulate anthocyanin biosynthesis appear to originate from photosynthetic tissues and can be transmitted to epidermal, mesophyll, and vascular cells [48,49]. Some DEGs were annotated in the "Ras signaling pathway". This indicated that various cellular processes, such as proliferation and apoptosis, were different in GA and RA. Liu et al. [50] reported that anthocyanins have anti-inflammatory and antioxidant effects in the treatment of diseases such as cancer. Some DEGs were annotated in the "Plant–pathogen interaction". This indicated that a series of genes related to adversity-stress responsiveness were downregulated in RA. Previous studies have reported

that anthocyanins not only promoted insect pollination but also protected plants from both biotic and abiotic stresses [51,52]. Based on these results, we could infer that the RA calyxes might be less sensitive to environmental stimulations and more tolerant of external stress conditions.

4.3. TFs Participating in Anthocyanin Accumulation

Two classes of genes regulate the biosynthesis of anthocyanins. One includes structural genes which encode enzymes that biosynthesize anthocyanins, and another includes the TFs that control the transcription of structural genes [24,53]. Transcription analysis indicated that MYB family genes accounted for the largest proportion among all annotated TFs. Previous studies have reported that the MYB family regulates anthocyanin-biosynthesis-related genes mainly in two ways. First, MYB proteins interact with bHLH and WD40 proteins to form a MBW protein complex and then activate structural genes. Second, independent MYB genes control EBGs to produce flavonols [54]. In our study, four MYB-related genes [*MYB1* (DN89812_c3_g1), *MYB82* (DN78431_c4_g4), *MYB113* (DN66235_c0_g2), and *SWR1-C* (DN94375_c1_g1)] and two bHLH genes [*PIF3* (*DN82050_c1_g1*) and *MYC2* (*DN102308_c2_g1*)] exhibited high correlations with differentially expressed LBGs. It was reported that the MYB-bHLH complex could regulate the expression of LBGs in *Arabidopsis* [13]. The MYB and bHLH TFs are usually expressed specifically in pigmented tissues. However, WD40 has been reported to provide a stable platform for the formation of the MBW complex, and its expression level is usually the same between pigmented tissues (due to anthocyanins) and non-pigmented tissues because of anthocyanins and non-pigmented tissues [55]. Studies on *Arabidopsis*, pear, and tea have indicated that the ability of the MYB-bHLH complex to activate the target gene is significantly higher than that of MYB alone [56,57]. When *SmMYB113* was co-expressed with *SmTT8* (*bHLH*) in an eggplant, the activation of *SmDFR* was significantly increased [58]. MYB82 could be co-expressed with specific bHLH and WD40 to form a MBW transcriptional activator complex to regulate trichome initiation or anthocyanin biosynthesis [59]. MYB82, as an important TF, caused anthocyanin accumulation in *Brassica rapa* and *Ananas comosus* var. *bracteatus* [60,61]. MYB1 was reported to activate the cascade of anthocyanin downstream regulators and structural genes in apple, celery, and rose and repress anthocyanin synthesis in *Fragaria* × *ananassa* [7,62–65]. In this study, the expression of MYB1 was decreased in the RA calyx. Therefore, we speculated that MYB1 in the calyx of RA functioned as the repressor in anthocyanin biosynthesis. In addition, some TFs were induced by hormones and stress; for example, GRAS (*DELLA*: *DN103810_c1_g1*), AP2/ERF-ERF (*PTI6*: *DN83232_c0_g2*), and C2C2-Dof (*CDF1*: *DN100839_c2_g1*) were significantly differentially expressed in the GA and RA calyxes. These TFs exhibited a high correlation with key candidate structural genes, which suggests that they could be stimulated by environmental changes to regulate biological processes, including anthocyanin-related pathways.

5. Conclusions

In summary, combined transcriptomic and metabolomics analyses were used to illustrate the relationship between key candidate genes and metabolites of anthocyanin biosynthetic pathways. A total of 202 DAMs and 4945 DEGs were identified in the calyxes of GA and RA. Furthermore, delphinidin 3, 5-diglucoside, delphinidin 3-O-glucoside, and malvidin 3-O-glucoside were the major components responsible for the purplish-red pigmentation in the calyx of RA. The integrative analysis of metabolomics and transcriptomics data revealed that LBGs [including *UFGT* (*DN92718_c0_g1*), three *ANSs* (*DN102834_c0_g1*, *DN93280_c6_g2*, and *DN90681_c0_g1*), and *DFR* (*DN103348_c0_g1*)] played an important role in anthocyanins accumulation, and the expression of key candidate LBGs could be regulated by the MYB-bHLH complex in calyxes of *S. japonicus*. In addition, many DAMs and DEGs were enriched in other pathways that could have a certain correlation with anthocyanin biosynthesis. These findings expand our knowledge of anthocyanin biosynthesis on color formation in *S. japonicus* calyx and offer useful gene resources for the molecular

breeding of S. japonicus with a purplish red calyx that could be of high ornamental value in the future.

Supplementary Materials: The following supporting information can be downloaded at: https://www.mdpi.com/article/10.3390/f14071413/s1, Figure S1: Differential metabolites analysis in GA and RA, Figure S2: Analysis of DEGs in GA and RA, Figure S3: Analysis of TFs in GA and RA, Figure S4: qPCR validation of transcript levels evaluated by RNA-seq., Figure S5: The co-expression analysis between metabolite accumulation and differential gene expression. Table S1: DAMs in the metabolomic analyses of GA vs. RA, Table S2: KEGG terms of DAMs, Table S3: DAMs enriched in anthocyanins-related pathways, Table S4: CleanData_QC summary, Table S5: The length distributions of assembled transcripts and unigenes, Table S6: The multiple mapped reads, Table S7: DEGs in the transcriptomic comparisons of GA vs. RA, Table S8: KEGG annotation classification frequencies, Table S9: The top 20 KEGG pathways, Table S10: DEGs encoding key enzymes involved in anthocyanin biosynthesis, Table S11: Differentially expressed transcription factors of GA vs. RA.

Author Contributions: Conceptualization, Y.J. and L.L.; Methodology, C.Z. and Y.Q.; Software, C.Q.; Validation, W.L. and Z.Z.; Supervision, H.Z. All authors have read and agreed to the published version of the manuscript.

Funding: This work was supported by the Subject of Key R & D Plan of Shandong Province (Major Scientific and Technological Innovation Project) "Mining and Accurate Identification of Forest Tree Germplasm Resources" (2021LZGC02303) and the Qingdao Agricultural University Doctoral Start-Up Fund (663/1121012), Qingdao Agricultural University Doctoral Start-Up Fund (663/1122010).

Data Availability Statement: The raw data can be available at https://www.ncbi.nlm.nih.gov/biosample?LinkName=bioproject_biosample_all&from_uid=542031 (accessed on 1 June 2023).

Conflicts of Interest: The authors declare no conflict of interest.

References

1. Zhang, J.J.; Li, B.; Gao, X.R.; Pan, X.Q.; Wu, Y.R. Integrating Transcriptomic and Metabolomic Analyses to Explore the Effect of Color Under Fruit Calyx on That of Fruit Apex in Eggplant (*Solanum melongena* L.). *Front. Genet.* **2022**, *13*, 889461. [CrossRef] [PubMed]
2. Timme, S.L. Liliaceae: Lily Family. In *Wildflowers of Mississippi*; University Press of Mississippi: Jackson, MS, USA, 2007; pp. 15–26.
3. Wróblewska, M.; Dolzblasz, A.; Zagórska-Marek, B.; Mendel, R. The role of ABC genes in shaping perianth phenotype in the basal angiosperm Magnolia. *Plant Biol.* **2016**, *18*, 230–238. [CrossRef] [PubMed]
4. Yoshida, K.; Ito, D.; Miki, N.; Kondo, T. Single-cell analysis clarifies mosaic color development in purple hydrangea sepal. *New Phytol.* **2021**, *229*, 3549–3557. [CrossRef]
5. Reyes-Luengas, A.; Salinas-Moreno, Y.; Ovando-Cruz, M.E.; Arteaga-Garibay, R.I.; Martinez-Pena, M.D. Analysis of phenolic acids and antioxidant activity of aqueous extracts of jamaica (*Hibiscus sabdariffa* L.) varieties with calyxes of different colors. *Agrociencia* **2015**, *49*, 277–290.
6. Saito, K.; Yonekura-Sakakibara, K.; Nakabayashi, R.; Higashi, Y.; Yamazaki, M.; Tohge, T.; Fernie, A.R. The flavonoid biosynthetic pathway in *Arabidopsis*: Structural and genetic diversity. *Plant Physiol. Biochem.* **2013**, *72*, 21–34. [CrossRef]
7. He, G.; Zhang, R.; Jiang, S.; Wang, H.; Ming, F. The MYB transcription factor RcMYB1 plays a central role in rose anthocyanin biosynthesis. *Hortic. Res.* **2023**, *10*, uhad080. [CrossRef]
8. Saigo, T.; Wang, T.; Watanabe, M.; Tohge, T. Diversity of anthocyanin and proanthocyanin biosynthesis in land plants. *Curr. Opin. Plant Biol.* **2020**, *55*, 93–99. [CrossRef]
9. Zhou, H.; Lin-Wang, K.; Wang, F.; Espley, R.V.; Ren, F.; Zhao, J.; Ogutu, C.; He, H.; Jiang, Q.; Allan, A.C. Activator-type R2R3-MYB genes induce a repressor-type R2R3-MYB gene to balance anthocyanin and proanthocyanidin accumulation. *New Phytol.* **2019**, *221*, 1919–1934. [CrossRef]
10. Fu, Z.; Jiang, H.; Chao, Y.; Dong, X.; Zhang, H. Three Paralogous R2R3-MYB Genes Contribute to Delphinidin-Related Anthocyanins Synthesis in *Petunia hybrida*. *J. Plant Growth Regul.* **2021**, *40*, 1687–1700. [CrossRef]
11. Mondal, S.K.; Roy, S. Genome-wide sequential, evolutionary, organizational and expression analyses of phenylpropanoid biosynthesis associated MYB domain transcription factors in *Arabidopsis*. *J. Biomol. Struct. Dyn.* **2018**, *36*, 1577–1601. [CrossRef]
12. Cavallini, E.; Matus, J.T.; Finezzo, L.; Zenoni, S.; Loyola, R.; Guzzo, F.; Schlechter, R.; Ageorges, A.; Arce-Johnson, P.; Tornielli, G.B. The Phenylpropanoid Pathway Is Controlled at Different Branches by a Set of R2R3-MYB C2 Repressors in Grapevine. *Plant Physiol.* **2015**, *167*, 1448–1470. [CrossRef] [PubMed]
13. Xu, W.; Dubos, C.; Lepiniec, L. Transcriptional control of flavonoid biosynthesis by MYB-bHLH-WDR complexes. *Trends Plant Sci.* **2015**, *20*, 176–185. [CrossRef] [PubMed]

14. Wang, X.; Wu, J.; Guan, M.; Zhao, C.; Zhao, Q. Arabidopsis MYB4 plays dual roles in flavonoid biosynthesis. *Plant J.* **2020**, *101*, 637–652. [CrossRef] [PubMed]
15. Zhang, F.; Gonzalez, A.; Zhao, M.; Payne, C.T.; Lloyd, A. A network of redundant bHLH proteins functions in all TTG1-dependentpathways of *Arabidopsis*. *Development* **2003**, *130*, 4859–4869. [CrossRef]
16. Liu, Z.; Zhang, Y.; Wang, J.; Li, P.; Zhao, C.; Chen, Y.; Bi, Y. Phytochrome-interacting factors PIF4 and PIF5 negatively regulate anthocyanin biosynthesis under red light in *Arabidopsis* seedlings. *Plant Sci.* **2015**, *238*, 64–72. [CrossRef]
17. Liu, Z.; Wang, Y.; Fan, K.; Li, Z.; Jia, Q.; Lin, W.; Zhang, Y. Phytochrome-Interacting Fcator 4 (PIF4) negatively regulates anthocyanin accumulation by inhibiting PAP1 transcription in *Arabidopsis* seedlings. *Plant Sci. Int. J. Exp. Plant Biol.* **2021**, *303*, 110788.
18. Deng, C.; Wang, J.; Lu, C.; Li, Y.; Kong, D.; Hong, Y.; Huang, H.; Dai, S. CcMYB6-1 and CcbHLH1, two novel transcription factors synergistically involved in regulating anthocyanin biosynthesis in cornflower. *Plant Physiol. Biochem.* **2020**, *151*, 271–283. [CrossRef]
19. Qin, J.; Zhao, C.; Wang, S.; Gao, N.; Wang, X.; Na, X.; Wang, X.; Bi, Y. PIF4-PAP1 interaction affects MYB-bHLH-WD40 complex formation and anthocyanin accumulation in *Arabidopsis*. *J. Plant Physiol.* **2022**, *268*, 153558. [CrossRef]
20. Matsui, K.; Umemura, Y.; Ohme-Takagi, M. AtMYBL2, a protein with a single MYB domain, acts as a negative regulator of anthocyanin biosynthesis in *Arabidopsis*. *Plant J.* **2008**, *55*, 954–967. [CrossRef]
21. Zhou, H.; Lin-Wang, K.; Wang, H.; Gu, C.; Dare, A.P.; Espley, R.V.; He, H.; Allan, A.C.; Han, Y. Molecular genetics of blood-fleshed peach reveals activation of anthocyanin biosynthesis by NAC transcription factors. *Plant J.* **2015**, *82*, 105–121. [CrossRef]
22. Zheng, T.; Tan, W.; Yang, H.; Zhang, L.E.; Li, T.; Liu, B.; Zhang, D.; Lin, H.; Qu, L.J. Regulation of anthocyanin accumulation via MYB75/HAT1/TPL-mediated transcriptional repression. *PLoS Genet.* **2019**, *15*, e1007993. [CrossRef] [PubMed]
23. Liu, H.; Chen, X.; Chen, H.; Huang, C. Transcriptome and Metabolome Analyses of the Flowers and Leaves of *Chrysanthemum dichrum*. *Front. Genet.* **2021**, *12*, 716163. [CrossRef] [PubMed]
24. Yu, F.; Xu, X.; Lin, S.; Peng, T.; Zeng, S. Integrated metabolomics and transcriptomics reveal flavonoids glycosylation difference in two Citrus peels. *Sci. Hortic.* **2022**, *292*, 110623. [CrossRef]
25. Zhang, L.; Tang, Z.M.; Zheng, H.; Zhong, C.H.; Zhang, Q. Comprehensive Analysis of Metabolome and Transcriptome in Fruits and Roots of Kiwifruit. *Int. J. Mol. Sci.* **2023**, *24*, 1299. [CrossRef] [PubMed]
26. Wang, X.Y.; Yu, S.; Liu, M.; Yang, Q.S.; Chen, X.Y. Twenty-three microsatellite loci for Styrax confusus and *Styrax japonicus* (Styracaceae). *Conserv. Genet. Resour.* **2009**, *2*, 51–54. [CrossRef]
27. Li, W.; Zhang, C.; Jiang, X.; Liu, Q.; Liu, Q.; Wang, K. De Novo Transcriptomic Analysis and Development of EST-SSRs for *Styrax japonicus*. *Forests* **2018**, *9*, 748. [CrossRef]
28. Li, W.; Xu, Z.; Zhang, C.; Jiang, X.; Wang, K.L. Transcriptomic Identification of Floral Transition and Development-Associated Genes in *Styrax japonicus*. *Forests* **2020**, *11*, 10. [CrossRef]
29. Zhang, J.; Wang, L.S.; Gao, J.M.; Shu, Q.Y.; Li, C.; Yao, J.; Hao, Q.; Zhang, J.J. Determination of anthocyanins and exploration of relationship between their composition and petal coloration in crape myrtle (*Lagerstroemia hybrid*). *J. Integr. Plant Biol.* **2008**, *50*, 581–588. [CrossRef]
30. Pekal, A.; Pyrzynska, K. Evaluation of Aluminium Complexation Reaction for Flavonoid Content Assay. *Food Anal. Methods* **2014**, *7*, 1776–1782. [CrossRef]
31. Qiu, J.; Xue, X.; Chen, F.; Li, C.; Bolat, N.; Wang, X.; Baima, Y.; Zhao, Q.; Zhao, D.; Ma, F. Quality evaluation of snow lotus (Saussurea): Quantitative chemical analysis and antioxidant activity assessment. *Plant Cell Rep.* **2010**, *29*, 1325–1337. [CrossRef]
32. Wang, X.G. Phenotypic Analysis of Different Varieties of Ornamental Carbapple. Master's Thesis, Hebei Normal University of Science & Technology, Qinhuangdao, China, 2018.
33. Qi, Y.Y.; Lou, Q.; Li, H.B.; Yue, J.; Liu, Y.L.; Wang, Y.J. Anatomical and biochemical studies of bicolored flower development in *Muscari latifolium*. *Protoplasma* **2013**, *250*, 1273–1281. [CrossRef] [PubMed]
34. Wang, Z.; Cui, Y.; Vainstein, A.; Chen, S.; Ma, H. Regulation of Fig (*Ficus carica* L.) Fruit Color: Metabolomic and Transcriptomic Analyses of the Flavonoid Biosynthetic Pathway. *Front. Plant Sci.* **2017**, *8*, 1990. [CrossRef] [PubMed]
35. Chen, W.; Gong, L.; Guo, Z.; Wang, W.; Zhang, H.; Liu, X.; Yu, S.; Xiong, L.; Luo, J. A Novel Integrated Method for Large-Scale Detection, Identification, and Quantification of Widely Targeted Metabolites: Application in the Study of Rice Metabolomics. *Mol. Plant* **2013**, *6*, 1769–1780. [CrossRef] [PubMed]
36. Hu, C.; Shi, J.; Quan, S.; Cui, B.; Kleessen, S.; Nikoloski, Z.; Tohge, T.; Alexander, D.; Guo, L.; Lin, H. Metabolic variation between japonica and indica rice cultivars as revealed by non-targeted metabolomics. *Sci. Rep.* **2014**, *4*, 5067. [CrossRef]
37. Cui, F.; Sui, N.; Duan, G.; Liu, Y.; Han, Y.; Liu, S.; Wan, S.; Li, G. Identification of Metabolites and Transcripts Involved in Salt Stress and Recovery in Peanut. *Front. Plant Sci.* **2018**, *9*, 217. [CrossRef] [PubMed]
38. Grabherr, M.G.; Haas, B.J.; Yassour, M.; Levin, J.Z.; Thompson, D.A.; Amit, I.; Adiconis, X.; Fan, L.; Raychowdhury, R.; Zeng, Q.; et al. Full-length transcriptome assembly from RNA-Seq data without a reference genome. *Nat. Biotechnol.* **2011**, *29*, 644–652. [CrossRef]
39. Sun, G.; Ju, Y.; Zhang, C.; Li, L.; Jiang, X.; Xie, X.; Lu, Y.; Wang, K.; Li, W. *Styrax japonicus* functional genomics: An efficient virus induced gene silencing (VIGS) system. *Hortic. Plant J.* 2023; *in press*. [CrossRef]
40. Oyama, K.I.; Yamada, T.; Ito, D.; Kondo, T.; Yoshida, K. Metal Complex Pigment Involved in the Blue Sepal Color Development of Hydrangea. *J. Agric. Food Chem.* **2015**, *63*, 7630–7635. [CrossRef]

41. Christian, K.R.; Jackson, J.C. Changes in total phenolic and monomeric anthocyanin composition and antioxidant activity of three varieties of sorrel (*Hibiscus sabdariffa*) during maturity. *J. Food Compos. Anal.* **2009**, *22*, 663–667. [CrossRef]
42. Salinas-Moreno, Y.; Zúñiga-Hernández, A.R.E.; Torre, L.B.J.-D.l.; Serrano-Altamirano, V.; Sánchez-Feria, C. Color en cálices de jamaica (*Hibiscus sabdariffa* L.) y su relación con características fisioquímicas de sus extractos acuosos. *Rev. Chapingo Ser. Hortic.* **2012**, *18*, 395–407. [CrossRef]
43. Wu, X.; Beecher, G.R.; Holden, J.M.; Haytowitz, D.B.; Prior, R.L. Concentrations of Anthocyanins in Common Foods in the United States and Estimation of Normal Consumption. *J. Agric. Food Chem.* **2006**, *54*, 4069–4075. [CrossRef]
44. Husain, A.; Chanana, H.; Khan, S.A.; Dhanalekshmi, U.M.; Ali, M.; Alghamdi, A.A.; Ahmad, A. Chemistry and Pharmacological Actions of Delphinidin, a Dietary Purple Pigment in Anthocyanidin and Anthocyanin Forms. *Front. Nutr.* **2022**, *9*, 746881. [CrossRef] [PubMed]
45. Lai, Y.S.; Li, S.; Tang, Q.; Li, H.X.; Chen, S.X. The Dark-Purple Tea Cultivar 'Ziyan' Accumulates a Large Amount of Delphinidin-Related Anthocyanins. *J. Agric. Food Chem.* **2016**, *64*, 2719–2726. [CrossRef] [PubMed]
46. Kerio, L.C.; Wachira, F.N.; Wanyoko, J.K.; Rotich, M.K. Characterization of anthocyanins in Kenyan teas: Extraction and identification. *Food Chem.* **2012**, *131*, 31–38. [CrossRef]
47. He, L.; Zhou, Y.; Wan, G.; Wang, W.; Zhang, N.; Yao, L. Antinociceptive effects of flower extracts and the active fraction from *Styrax japonicus*. *J. Ethnopharmacol.* **2022**, *284*, 114779. [CrossRef] [PubMed]
48. Das, P.K.; Geul, B.; Choi, S.B.; Yoo, S.D.; Park, Y. Photosynthesis-dependent anthocyanin pigmentation in *Arabidopsis*. *Plant Signal. Behav.* **2011**, *6*, 23–25. [CrossRef] [PubMed]
49. Li, Y.; Lei, W.; Zhou, Z.; Li, Y.; Zhang, D.; Lin, H. Transcription factor GLK1 promotes anthocyanin biosynthesis via an MBW complex-dependent pathway in *Arabidopsis thaliana*. *J. Integr. Plant Biol.* **2023**, *65*, 1521–1535. [CrossRef] [PubMed]
50. Liu, J.; Zhou, H.; Song, L.; Yang, Z.; Qiu, M.; Wang, J.; Shi, S. Anthocyanins: Promising Natural Products with Diverse Pharmacological Activities. *Molecules* **2021**, *26*, 3807. [CrossRef]
51. Mackon, E.; Jeazet Dongho Epse Mackon, G.C.; Ma, Y.; Haneef Kashif, M.; Ali, N.; Usman, B.; Liu, P. Recent Insights into Anthocyanin Pigmentation, Synthesis, Trafficking, and Regulatory Mechanisms in Rice (*Oryza sativa* L.) Caryopsis. *Biomolecules* **2021**, *11*, 394. [CrossRef]
52. Naing, A.H.; Kim, C.K. Abiotic stress-induced anthocyanins in plants: Their role in tolerance to abiotic stresses. *Physiol. Plant.* **2021**, *172*, 1711–1723. [CrossRef]
53. Zhang, H.; Chen, J.; Peng, Z.; Shi, M.; Liu, X.; Wen, H.; Jiang, Y.; Cheng, Y.; Xu, J.; Zhang, H. Integrated Transcriptomic and Metabolomic analysis reveals a transcriptional regulation network for the biosynthesis of carotenoids and flavonoids in 'Cara cara' navel Orange. *BMC Plant Biol.* **2021**, *21*, 29. [CrossRef]
54. Petroni, K.; Tonelli, C. Recent advances on the regulation of anthocyanin synthesis in reproductive organs. *Plant Sci. Int. J. Exp. Plant Biol.* **2011**, *181*, 219–229. [CrossRef] [PubMed]
55. Koes, R.; Verweij, W.; Quattrocchio, F. Flavonoids: A colorful model for the regulation and evolution of biochemical pathways. *Trends Plant Sci.* **2005**, *10*, 236–242. [CrossRef]
56. Sun, B.; Zhu, Z.; Cao, P.; Chen, H.; Chen, C.; Zhou, X.; Mao, Y.; Lei, J.; Jiang, Y.; Meng, W.; et al. Purple foliage coloration in tea (*Camellia sinensis* L.) arises from activation of the R2R3-MYB transcription factor CsAN1. *Sci. Rep.* **2016**, *6*, 32534. [CrossRef] [PubMed]
57. Yao, G.; Ming, M.; Allan, A.C.; Gu, C.; Li, L.; Wu, X.; Wang, R.; Chang, Y.; Qi, K.; Zhang, S.; et al. Map-based cloning of the pear gene MYB114 identifies an interaction with other transcription factors to coordinately regulate fruit anthocyanin biosynthesis. *Plant J.* **2017**, *92*, 437–451. [CrossRef]
58. Zhou, L.; He, Y.; Li, J.; Liu, Y.; Chen, H. CBFs Function in Anthocyanin Biosynthesis by Interacting with MYB113 in Eggplant (*Solanum melongena* L.). *Plant Cell Physiol.* **2020**, *61*, 416–426. [CrossRef] [PubMed]
59. Zheng, K.; Wang, X.; Wang, Y.; Wang, S. Conserved and non-conserved functions of the rice homologs of the Arabidopsis trichome initiation-regulating MBW complex proteins. *BMC Plant Biol.* **2021**, *21*, 234.
60. Zhou, B.; Leng, J.; Ma, Y.; Fan, P.; Li, Y.; Yan, H.; Xu, Q. BrmiR828 Targets BrPAP1, BrMYB82, and BrTAS4 Involved in the Light Induced Anthocyanin Biosynthetic Pathway in *Brassica rapa*. *Int. J. Mol. Sci.* **2020**, *21*, 4326. [CrossRef]
61. Zhou, X.; Xue, Y.; Mao, M.; He, Y.; Adjei, M.O.; Yang, W.; Hu, H.; Liu, J.; Feng, L.; Zhang, H.; et al. Metabolome and transcriptome profiling reveals anthocyanin contents and anthocyanin-related genes of chimeric leaves in *Ananas comosus* var. *bracteatus*. *BMC Genom.* **2021**, *22*, 331. [CrossRef]
62. Aharoni, A.; De Vos, C.H.; Wein, M.; Sun, Z.; Greco, R.; Kroon, A.; Mol, J.N.; O'Connell, A.P. The strawberry FaMYB1 transcription factor suppresses anthocyanin and flavonol accumulation in transgenic tobacco. *Plant J. Cell Mol. Biol.* **2001**, *28*, 319–332. [CrossRef]
63. Ban, Y.; Honda, C.; Hatsuyama, Y.; Igarashi, M.; Bessho, H.; Moriguchi, T. Isolation and functional analysis of a MYB transcription factor gene that is a key regulator for the development of red coloration in apple skin. *Plant Cell Physiol.* **2007**, *48*, 958–970. [CrossRef]

64. Espley, R.V.; Hellens, R.P.; Putterill, J.; Stevenson, D.E.; Kutty-Amma, S.; Allan, A.C. Red colouration in apple fruit is due to the activity of the MYB transcription factor, MdMYB10. *Plant J. Cell Mol. Biol.* **2007**, *49*, 414–427. [CrossRef] [PubMed]
65. Feng, K.; Xing, G.M.; Liu, J.X.; Wang, H.; Tan, G.F.; Wang, G.L.; Xu, Z.S.; Xiong, A.S. AgMYB1, an R2R3-MYB factor, plays a role in anthocyanin production and enhancement of antioxidant capacity in celery. *Veg. Res.* **2021**, *1*, 2. [CrossRef]

Disclaimer/Publisher's Note: The statements, opinions and data contained in all publications are solely those of the individual author(s) and contributor(s) and not of MDPI and/or the editor(s). MDPI and/or the editor(s) disclaim responsibility for any injury to people or property resulting from any ideas, methods, instructions or products referred to in the content.